Journal of Materials Chemistry A

PAPER

View Article Online
View Journal | View Issue

Cite this: J. Mater. Chem. A, 2016, 4, 6350

Facile synthesis of hierarchical porous Co_3O_4 nanoboxes as efficient cathode catalysts for Li–O_2 batteries†

Jian Zhang,‡[ab] Zhiyang Lyu,‡[b] Feng Zhang,‡[bc] Liangjun Wang,[d] Peng Xiao,[b] Kaidi Yuan,[d] Min Lai[a] and Wei Chen*[bde]

Received 8th March 2016
Accepted 10th April 2016

DOI: 10.1039/c6ta01995a

www.rsc.org/MaterialsA

Rechargeable Li–O_2 batteries with remarkably high theoretical energy densities have attracted extensive attention. However, to enable Li–O_2 batteries for practical applications, numerous challenges need to be overcome, *e.g.* high overpotential, low rate capability, and poor cycling stability. The key factor to tackle these issues is to develop highly-efficient cathode catalysts. Moreover, cathode catalysts with a porous structure and large surface area are favorable in Li–O_2 batteries. In this paper, hierarchical porous Co_3O_4 nanoboxes with well-defined interior voids, functional shells and a large surface area have been facilely synthesized *via* an ion exchange reaction between Prussian blue analogue nanocubic precursors and OH^- at a low temperature (60 °C). The obtained products possess hierarchical pore sizes and an extremely large surface area (272.5 m^2 g^{-1}), which provide more catalytically active sites to promote the oxygen reduction reaction (ORR) and oxygen evolution reaction (OER) as a Li–O_2 battery cathode, as well as facilitating the diffusion of oxygen and the electrolyte. The hierarchical porous Co_3O_4 nanobox cathode shows enhanced discharge capacity, reduced overpotential, improved rate performance and cycle stability, in comparison with the EC-300J carbon cathode. The superb performance of the hierarchical porous Co_3O_4 nanoboxes, together with the facile fabrication approach, presents an alternative method to develop advanced cathode catalysts for Li–O_2 batteries.

1. Introduction

Excessive use of fossil fuels has caused serious environmental problems, such as air pollution and global warming, *etc.*[1] Electric vehicles hold the potential for reducing the use of fossil fuels, cutting carbon dioxide emissions, and improving air quality. Power supply is one of the key parts for realizing the wide application of electric vehicles. Therefore, many efforts have been devoted to the development of high capacity energy storage systems.[2–6] Rechargeable Li–O_2 batteries with remarkably high theoretical energy densities have attracted extensive attention.[7,8] The theoretical energy density of Li–O_2 batteries is about 3500 W h kg^{-1}, which is about 4 to 6 times higher than that of conventional Li-ion batteries.[9] However, Li–O_2 batteries still suffer from many challenges for practical applications, such as electrolyte instability, poor cycle stability and high overpotential.[10–12] One effective way to overcome these problems is to develop highly-efficient cathode catalysts. Many catalysts, such as noble metals and metal oxides,[13–16] non-noble metal oxides,[17–19] and carbon-based materials[20–22] have been developed as cathode catalysts for Li–O_2 batteries in order to improve battery performance.

Hollow-structured catalysts with well-defined interior voids, functional shells and large surface areas are favorable in the application of Li–O_2 batteries, regardless of what type of catalysts are developed. They can facilitate the effective transportation of oxygen and the electrolyte and provide sufficient catalytically active sites to promote the oxygen reduction reaction (ORR) and oxygen evolution reaction (OER), thereby leading to improved battery performance.[23,24] Even mixed with carbon additives to prepare the cathodes, a well-defined hollow structure can act as a framework to build fine porous conducting matrixes, which ensures easy infiltration of the electrolyte and the diffusion of oxygen. The presence of the hollow structure can also minimize undesirable clogging of the cathode; thereby, dramatically improving the cycle stability of the Li–O_2 batteries. Prussian blue analogues (PBAs) with

[a]School of Physics and Optoelectronic Engineering, Nanjing University of Information Science & Technology, Nanjing 210044, Jiangsu, China
[b]Department of Chemistry, National University of Singapore, 3 Science Drive 3, 117543, Singapore. E-mail: phycw@nus.edu.sg
[c]School of Chemistry and Chemical Engineering, Nanjing University, Nanjing 210046, China
[d]Department of Physics, National University of Singapore, 2 Science Drive 3, 117542 Singapore
[e]National University of Singapore (Suzhou) Research Institute, 377 Lin Quan Street, Suzhou Industrial Park, Jiangsu Prov. 215123, China

† Electronic supplementary information (ESI) available. See DOI: 10.1039/c6ta01995a

‡ These authors contributed equally to this work.

controlled morphology have been recognized as promising precursors to synthesize porous and hollow metal oxides,[25–28] such as Fe_2O_3, $Fe_xCo_{3-x}O_4$, CuO/Cu_2O. Among them, Co–Mn–O nanocubes and hierarchical porous δ-MnO_2 nanoboxes have been demonstrated as efficient cathode catalysts for Li–O_2 batteries.[29,30]

Co_3O_4 has been demonstrated as a potential cathode catalyst for rechargeable Li–O_2 batteries due to its high catalytic ability, controllable size and morphology, and various approaches have been developed to synthesize Co_3O_4-based catalysts.[31–34] However, most of the existing processes for the synthesis of Co_3O_4-based catalysts are based on hydrothermal and calcination methods which result in final products with small surface areas and non-porous structures. There has been limited success in the facile synthesis of hollow Co_3O_4 materials which can act as good cathode catalysts for Li–O_2 batteries.

In this work, we developed a facile method to synthesize porous Co_3O_4 nanoboxes *via* an ion exchange reaction between PBA nanocubic precursors and OH^- at a low temperature (60 °C). The as-synthesized Co_3O_4 nanoboxes possessed a hierarchical porous structure and large surface area up to 272.5 m^2 g^{-1}. When employed as the cathode catalyst for Li–O_2 batteries, the porous Co_3O_4 nanoboxes showed high catalytic activity towards both ORR and OER with a reduced overpotential up to 300 mV, and presented enhanced capacity and improved rate performance. The synergistic effects of large specific surface area, porous structure, and high electrocatalytic activity of the porous Co_3O_4 nanobox electrode ensured a Li–O_2 battery with excellent cycle stability (168 cycles at a limited capacity of 500 mA h g^{-1} and 124 cycles at 1000 mA h g^{-1}).

2. Experimental

2.1 Synthesis procedures

Synthesis of PBA precursors. The nanocube-like PBA precursors were synthesized *via* a modified self-assembly method.[35,36] Typically, 0.6 mmol (174 mg) of cobalt nitride and 1.34 mmol (397 mg) of sodium citrate were dissolved in 20 mL of DI water to form a transparent solution A. In the meantime, 0.4 mmol (132 mg) of $K_3[Fe(CN)_6]$ was dissolved into 20 mL of DI water to form a clear solution B. Then, solution A and B were mixed quickly and stirred for 5 min. The mixed solution was kept at room temperature for 24 h. The resulting white precipitate was collected by centrifugation and washed several times with absolute ethanol, then dried at 80 °C overnight.

Synthesis of Co_3O_4 nanoboxes. Porous Co_3O_4 nanoboxes were obtained by the reaction of Co–Fe PBAs with NaOH at a low temperature. In a typical synthesis, 20 mg of the as-prepared Co–Fe PBA nanocubes were dispersed into 20 mL of ethanol and ultrasonicated for 10 min to form a homogeneous suspension. Then, 20 and 40 mL of 0.025 M NaOH was added to this suspension. After stirring for 5 min, the mixed solution was transferred to a 100 mL Teflon-lined stainless-steel autoclave and kept at 60 °C for 30 min. The final products were collected and washed with absolute ethanol and DI water several times, and finally dried in an oven at 80 °C. To understand the formation process and optimize the reaction conditions, different reaction times (30 min and 120 min) and reaction temperatures (room temperature, 60 °C and 100 °C), as well as NaOH solutions with different concentrations (0.01 M, 0.05 M and 0.1 M) were used to synthesize a series of Co_3O_4.

2.2 Instruments for characterization

The morphology of the as-prepared samples was examined by scanning electron microscopy (SEM) on a JEOL JSM 6700F and transmission electron microscopy (TEM) on a JEOL 2010 microscope. The composition of the samples was analyzed by energy-dispersive X-ray spectroscopy (EDX) attached to the TEM instrument. The X-ray diffraction (XRD) patterns of the samples were collected from a PANalytical Empyren DY 708 diffractometer with Cu radiation (Cu Kα = 0.15406 nm). The Brunauer–Emmett–Teller (BET) surface area was measured by nitrogen sorption at 77 K on a surface area & pore size analyzer (NOVA 2200e). X-ray photoelectron spectroscopy (XPS) analyses were obtained on an XR 50 HP X-ray source and Phoibos HSA3500 analyzer.

2.3 Li–O_2 cell assembly and battery test

Generally, the catalyst slurry was prepared by mixing 40% catalyst with 50% Ketjenblack EC-300J (EC-300J) carbon (Cabot Carbon Ltd) and 10% polytetrafluoroethylene (PTFE), or 90% EC-300J carbon with 10% PTFE. The air cathodes were fabricated by coating the catalyst slurry on a carbon paper current collector homogenously. The mass loading of the slurry on the cathode was about 0.8–1.2 mg cm^{-2}, and the discharge capacity was calculated based on the total weight of the catalyst and carbon additives. All the Li–O_2 batteries were assembled by using coin cells in a glove box under an argon atmosphere. Glass fiber membranes were used as the separator and 1 M lithium trifluoromethanesulfonate/tetraethylene glycol dimethyl ether ($LiCF_3SO_3$/TEGDME) was used as the electrolyte. Galvanostatic discharge–charge tests of the Li–O_2 battery were carried out on a LAND multi-channel battery testing system.

3. Results and discussions

3.1 Synthesis, morphological, structural characterization

The fabrication of the hollow Co_3O_4 nanoboxes was carried out through a two-step route. Firstly, nanosized PBA precursors were synthesized through a self-assembly solution method.[35,36] The morphology of the as-synthesized precursors was examined by SEM and TEM and is shown in Fig. 1a and b. These precursors presented a well-defined cubic shape with an average size of 150–250 nm and smooth facets. The XRD pattern (Fig. 1c) evidenced that the precursors were $KCo[Fe(CN)_6]\cdot 3H_2O$ instead of $Co_3[Fe(CN)_6]_2\cdot nH_2O$, consistent with the previous report.[35] The existence of the K element was also confirmed by EDX and XPS measurements, as shown in Fig. S1a and S2a.† In the next step, the as-prepared precursors were mixed with NaOH solution to conduct the ion exchange reaction. In the NaOH solution, the ion exchange reaction happened as described below:

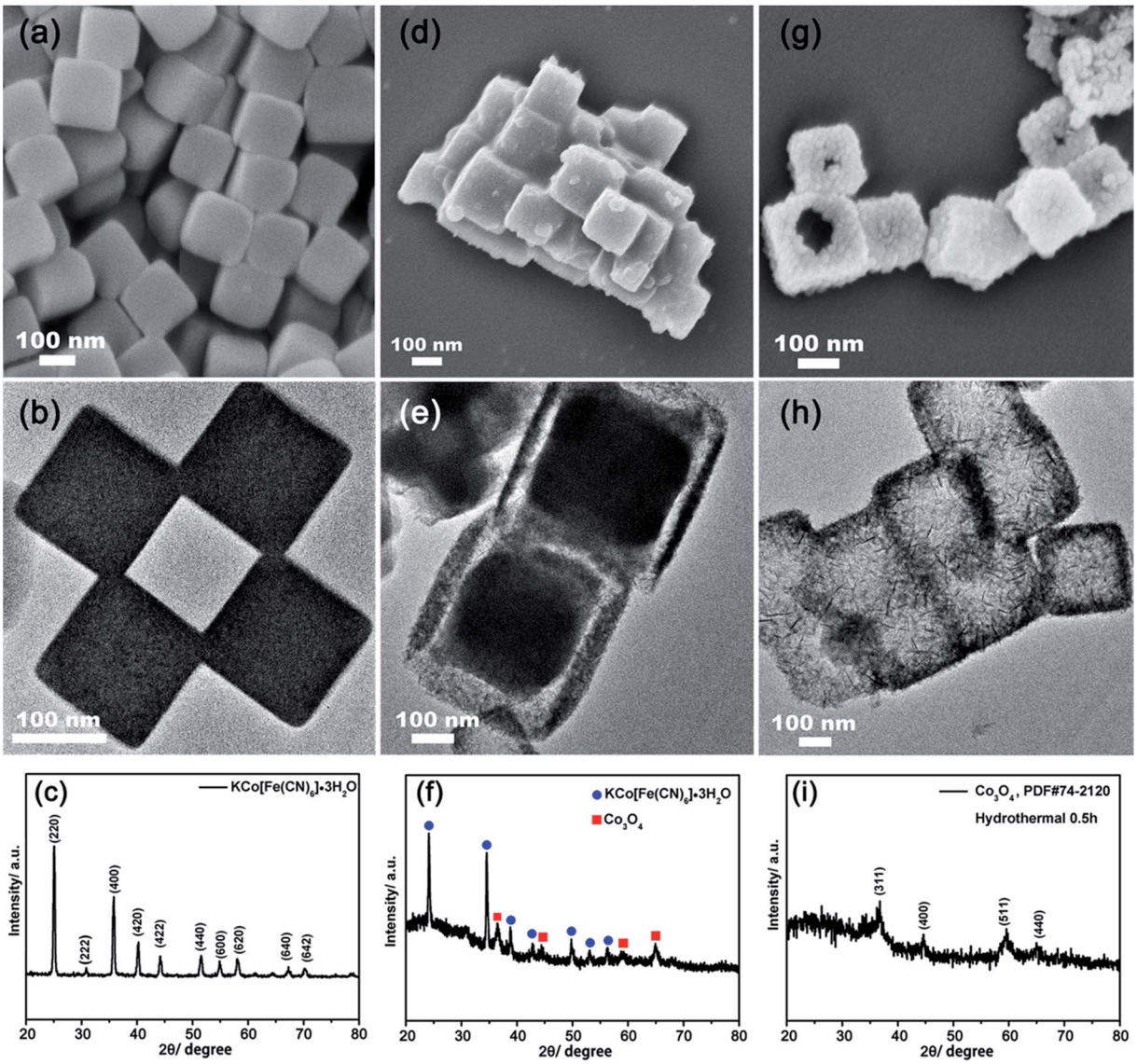

Fig. 1 SEM images (a, d and g), TEM images (b, e and h) and XRD patterns (c, f and i) of the obtained nanocube-like PBA precursors (a–c), yolk-shelled nanoboxes (d–f) and hierarchical porous Co_3O_4 nanoboxes (g–i).

$$KCo[Fe(CN)_6](s) + 2OH^-(aq) \rightarrow Co(OH)_2(s) + Fe(CN)_6^{3-} + K^+.$$

It was found that when 20 mL of 0.025 M NaOH solution was used, a yolk-shelled structural compound was obtained as shown in Fig. 1d and e. The XRD pattern (Fig. 1f) indicated that the compound was a mix of ingredients comprising Co_3O_4 and $KCo[Fe(CN)_6]\cdot 3H_2O$. On increasing the amount of 0.025 M NaOH solution to 40 mL, perfect hollow nanoboxes were obtained, as shown in Fig. 1g and h. The as-prepared nanoboxes analyzed by XRD were indexed to Co_3O_4 (PDF #74-2120) instead of $Co(OH)_2$ (Fig. 1i). This was possibly due to the fact that $Co(OH)_2$ can be easily oxidized by the dissolved oxygen during the reaction process.[37,38] Therefore, it can be proposed that the ion exchange reaction firstly took place at the interface between the solid PBA nanocubic precursors and NaOH solution when the concentration of NaOH was 0.025 M, and a thin layer of Co_3O_4 was formed. With the reaction proceeded, the solid $KCo[Fe(CN)_6]\cdot 3H_2O$ continued dissolve and diffuse outward to react with OH^- to form $Co(OH)_2$. Subsequently, it was oxidized by oxygen to form Co_3O_4.[39] If the amount of OH^- was adequate, the ion exchange reaction proceeded until all the PBAs were consumed and well-defined nanoboxes were finally formed (Fig. 1g and h). Otherwise, an incomplete ion exchange reaction took place and a yolk-shelled structural compound was obtained (Fig. 1d and e). The ion exchange reaction was also evidenced by EDX and XPS analysis. As shown in Fig. S1 and S2,† the characteristic peaks of K and Fe in the EDX spectrum and dominant K 2p, Fe 2p and N 1s peaks in the XPS spectra disappeared after adding 40 mL of 0.025 M NaOH, indicating the removal of K^+ and $[Fe(CN)_6]^{3-}$. The XPS measurements (Fig. S3†) further confirmed the formation of Co_3O_4. The two peaks at 794.7 and 779.5 eV correspond to the Co $2p_{3/2}$ and Co $2p_{1/2}$ of Co_3O_4, which were in good agreement with previous reports.[40,41]

The HR-TEM of the as-prepared hollow Co_3O_4 nanoboxes is shown in Fig. 2. The surface of the nanoboxes is dominated by the assembly of nanosheets and nanoneedles (Fig. 2b and c). A clear lattice spacing of 0.202 nm was also observed in the high-resolution TEM image (Fig. 2d), in good agreement with the inter-plane spacing of the (400) plane of Co_3O_4 (PDF #74-2120). The SAED pattern (Fig. 2a inset) showed that the Co_3O_4 was polycrystalline. The specific surface area and porosity of the Co_3O_4 nanoboxes were determined by N_2 adsorption–desorption measurements. A type IV nitrogen adsorption–desorption isotherm with a H3-shaped hysteresis loop is shown in Fig. 2e. The BET specific surface area of the porous Co_3O_4 nanoboxes was up to 272.5 m^2 g^{-1}. To our knowledge, this is one of the largest surface areas reported among Co_3O_4 materials.[34,37,42] The pore size distribution calculated from the Barrett–Joyner–Halenda (BJH) method is shown in the inset of Fig. 2e. A wide range of pore sizes from 20 to 140 nm was observed. The sharp peak centred at about 60 nm was related to the hollow structure of the nanoboxes, and the mesopores existing in the porous Co_3O_4 nanoboxes resulted from the accumulated pores of inter-nanoboxes and inter-nanosheets on the surface of the nanoboxes. The pore volume of the porous Co_3O_4 nanoboxes was about 0.63 cm^3 g^{-1}.

We also investigated the correlation of the morphology of Co_3O_4 with the reaction conditions such as reaction time, reaction temperature and the NaOH concentration, as shown in Fig. 3. It can be seen in Fig. 3a that similar Co_3O_4 nanoboxes were obtained when the reaction time was extended to 120 min, which indicated that no further reaction took place after the completion of the ion exchange reaction. Fig. 3b and c show the products obtained at room temperature and 100 °C, respectively. When mixing the PBA nanocubic precursors with NaOH at room temperature, no obvious change in the PBA nanocubic precursors was observed (Fig. 3b), indicating that no ion exchange reaction occurred at room temperature. However, when the temperature was increased to 100 °C, Co_3O_4 nanoboxes formed *via* the assembly of small nanoparticles were observed, as shown in Fig. 3c. These results suggested that temperature was one of the dominant factors for the ion exchange reaction. At room temperature, the thermal energy was not sufficient to drive the ion exchange reaction; while a high temperature (100 °C) can accelerate the reaction and lead to the formation of localized nanoparticles. The concentration of NaOH also had a crucial effect on the ion exchange reaction. Both the PBAs and $Co(OH)_2$ were insoluble in water. The proceeding of the ion exchange reaction was attributed to the high concentration of NaOH, which promoted the forward reaction to form the $Co(OH)_2$. As shown in Fig. 3d, if the concentration was relatively low (0.01 M), negligible change in the PBA precursors was observed. When the concentration of NaOH was increased to 0.05 M, a hollow structure was maintained. However, the surface of the nanoboxes was partially damaged (Fig. 3e), which may be due to the rapid ion exchange reaction rate. At the NaOH concentration of 0.1 M, the inward diffusion of OH^- and the rate of ion exchange reaction were significantly accelerated, thereby completely destroying the nanobox structure and causing the formation of scattered nanoparticles (Fig. 3f). These results indicated that the key to obtaining the hollow Co_3O_4 nanoboxes was the precise control of the reaction temperature and the concentration of the alkaline solution.

3.2 Battery testing

The battery performance of the porous Co_3O_4 nanoboxes catalyst was evaluated by galvanostatic discharge–charge measurements in coin-cell type Li–O_2 batteries. EC-300J carbon was used as both the conductive additive and the reference cathode for comparison. Fig. 4a shows the first discharge–charge profiles of the Li–O_2 cells with porous Co_3O_4 nanoboxes and EC-300J carbon electrodes at the current density of 0.08 mA cm^{-2}. In the first discharge process, the porous Co_3O_4 nanobox electrode

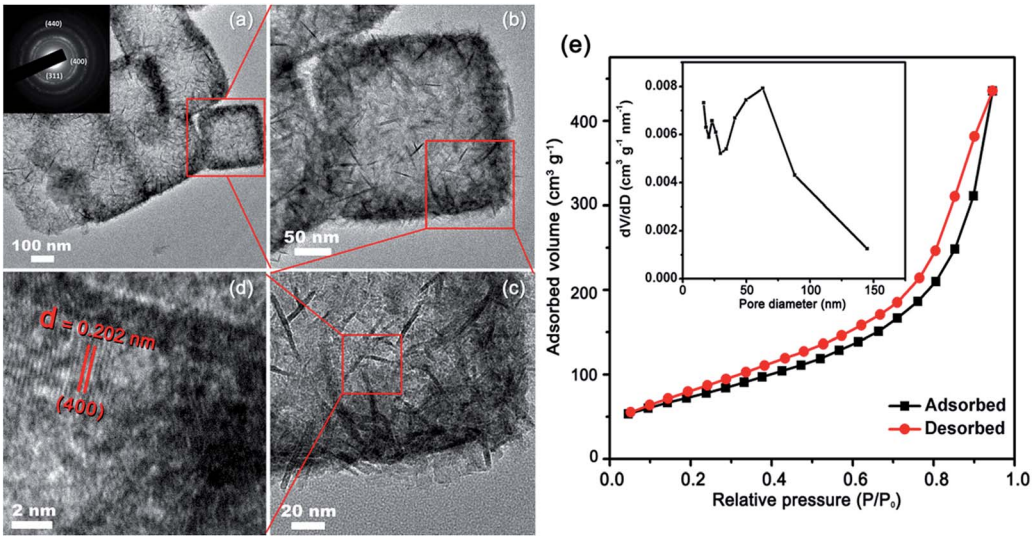

Fig. 2 HR-TEM images (a–d) of hierarchical porous Co_3O_4 nanoboxes, inset in (a) is SAED pattern; (e) nitrogen adsorption–desorption isotherms and pore size distribution (inset) of the hierarchical porous Co_3O_4 nanoboxes.

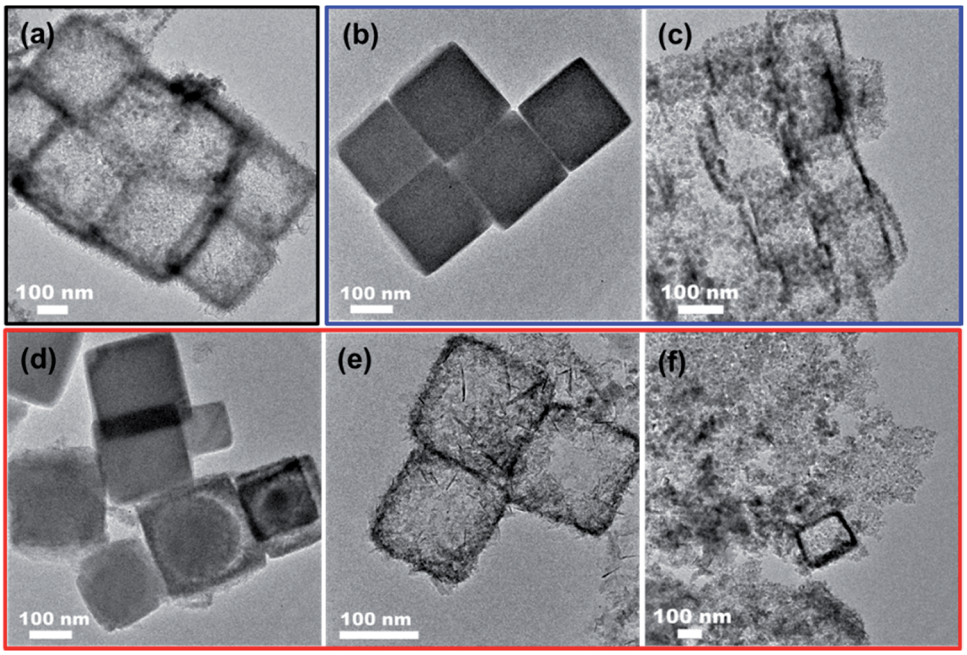

Fig. 3 TEM images of the final products under various experimental conditions: (a) react for 120 min; (b) at room temperature; (c) at 100 °C; (d–f) with 40 mL 0.01 M, 0.05 M and 0.1 M NaOH, respectively.

delivered a specific capacity of about 4032 mA h g^{-1}, which was much larger than that of the EC-300J carbon electrode (2535 mA h g^{-1}). The enhanced capacity was attributed to the large surface area of the porous Co_3O_4 nanobox catalyst, which provided sufficient space to afford the deposition of Li_2O_2. In addition, the relatively higher catalytic activity of the porous

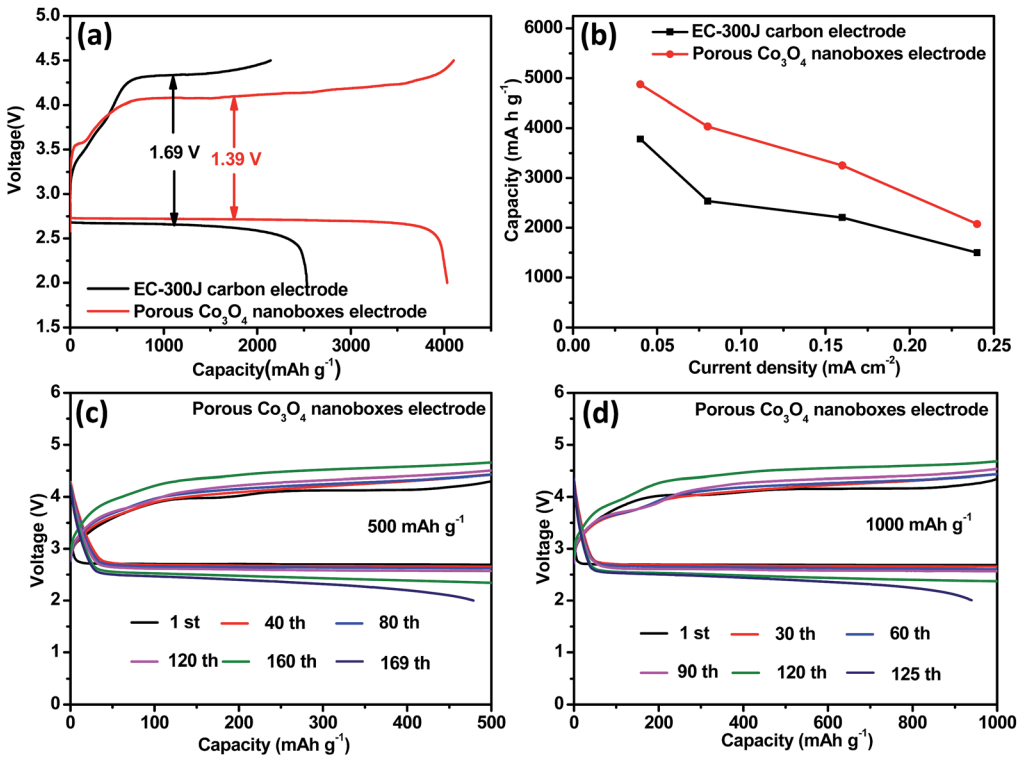

Fig. 4 (a) First discharge–charge curves of Li–O_2 batteries with the hierarchical porous Co_3O_4 nanobox and EC-300J carbon electrodes at 0.08 mA cm^{-2}; (b) discharge capacity of Li–O_2 battery cells with different electrodes at various current densities; (c) and (d) cyclic performance of the hierarchical porous Co_3O_4 nanobox electrode at 0.16 mA cm^{-2} with limited capacities of (c) 500 mA h g^{-1} and (d) 1000 mA h g^{-1}, respectively.

Co_3O_4 nanobox catalyst also promoted the ORR. More importantly, the high catalytic activity of the porous Co_3O_4 nanoboxes gave rise to an increased discharge potential and reduced charge potential of the Li–O_2 battery. As can be seen in Fig. 4a, the voltage gap of the battery with the porous Co_3O_4 nanoboxes was about 1.39 V, which was about 300 mV lower than that of the EC-300J electrode. The reduced overpotential meant enhanced round-trip efficiency (the ratio of discharge to charge voltage). As shown in Fig. 4b and S4a,† the rate performance of the porous Co_3O_4 nanoboxes was further investigated at the current densities of 0.04, 0.16 and 0.24 mA cm^{-2}, respectively. The batteries with porous Co_3O_4 nanobox electrodes exhibited capacities of 4876 mA h g^{-1} at 0.04 mA cm^{-2}, 3250 mA h g^{-1} at 0.16 mA cm^{-2} and 2075 mA h g^{-1} at 0.24 mA cm^{-2}. It should be noted that these capacities were much higher than those of the EC-300J carbon electrodes at the same current density (Fig. 4b and S4b†). The porous Co_3O_4 nanobox electrode also exhibited better capacity retention than the EC-300J carbon electrode under all investigated current densities (Fig. S4c†). These results further indicated that the porous Co_3O_4 nanobox electrode had better rate performance. The improved rate performance of the porous Co_3O_4 nanobox electrode was attributed to the porous structure facilitating the diffusion of oxygen and electrolyte during the discharge process. In addition, the high catalytic activity of the catalysts, which can promote the sluggish ORR even at high current densities, was also beneficial to improve the battery performance. To investigate the stability of the porous Co_3O_4 nanobox electrode, the long-term performance of the porous Co_3O_4 nanobox electrode was evaluated following a widely used method by limiting the discharge capacity.[23,43] When the discharge potential dropped below 2.0 V, we considered the cells to have failed. Fig. 4c and d show the selected cycled voltage profiles of the batteries with porous Co_3O_4 nanobox electrodes at the current density of 0.16 mA cm^{-2} with limited capacities of 500 mA h g^{-1} and 1000 mA h g^{-1}, respectively. As can be seen in Fig. 4c, there was no loss of discharge capacity until the 168th cycle with a limited capacity of 500 mA h g^{-1}. When increasing the curtailing capacity to 1000 mA h g^{-1}, the battery with the porous Co_3O_4 nanobox electrode could still be cycled for 125 cycles (Fig. 4d). In contrast, as shown in Fig. S5,† the cycle numbers of the EC-300J electrodes decreased to 20 and 11 with the limited capacities of 500 mA h g^{-1} and 1000 mA h g^{-1}, respectively, which were much smaller than those of the porous Co_3O_4 nanobox electrode. These results reveal that the porous Co_3O_4 nanobox electrode had excellent cycle stability.

4. Conclusion

In conclusion, we have developed a facile and controllable method to synthesize porous Co_3O_4 nanoboxes at a low temperature (60 °C) by using Prussian blue analogues as the precursor. The correlation between the morphology and the experimental conditions was also investigated in detail. The obtained products possessed hierarchical pores and an extremely large surface area (272.5 m^2 g^{-1}), which favour oxygen transportation and provide more catalytically active sites to promote ORR and OER. By using the porous Co_3O_4 nanoboxes as the cathode catalyst, the Li–O_2 batteries showed improved battery performance with higher discharge capacity, lower overpotential, enhanced rate performance and superior cycle stability. The facile fabrication method reported here also represented an alternative to develop metal oxide nanomaterials for potential applications in Li–O_2 batteries, as well as other applications such as supercapacitors and Li-ion batteries.

Acknowledgements

The authors acknowledge the financial support from the Singapore MOE grant R143-000-593-112 and China Scholarship Council.

Notes and references

1 I. Dincer, *Renewable Sustainable Energy Rev.*, 2000, **4**, 157–175.
2 H. Zhang, S. Jing, Y. Hu, H. Jiang and C. Li, *J. Power Sources*, 2016, **307**, 214–219.
3 Y. Dai, L. Chen, V. Babayan, Q. Cheng, P. Saha, H. Jiang and C. Li, *J. Mater. Chem. A*, 2015, **3**, 21337–21342.
4 H. Jiang, H. Zhang, Y. Fu, S. Guo, Y. Hu, L. Zhang, Y. Liu, H. Liu and C. Li, *ACS Nano*, 2016, **10**, 1648–1654.
5 C. Yuan, H. B. Wu, Y. Xie and X. W. Lou, *Angew. Chem., Int. Ed.*, 2014, **53**, 1488–1504.
6 J. Jiang, Y. Li, J. Liu, X. Huang, C. Yuan and X. W. Lou, *Adv. Mater.*, 2012, **24**, 5166–5180.
7 P. G. Bruce, S. A. Freunberger, L. J. Hardwick and J. M. Tarascon, *Nat. Mater.*, 2012, **11**, 19–29.
8 A. C. Luntz and B. D. McCloskey, *Chem. Rev.*, 2014, **114**, 11721–11750.
9 R. Black, S. H. Oh, J.-H. Lee, T. Yim, B. Adams and L. F. Nazar, *J. Am. Chem. Soc.*, 2012, **134**, 2902–2905.
10 Y. Y. Shao, F. Ding, J. Xiao, J. Zhang, W. Xu, S. Park, J. G. Zhang, Y. Wang and J. Liu, *Adv. Funct. Mater.*, 2013, **23**, 987–1004.
11 G. Girishkumar, B. McCloskey, A. C. Luntz, S. Swanson and W. Wilcke, *J. Phys. Chem. Lett.*, 2010, **1**, 2193–2203.
12 F. Y. Cheng and J. Chen, *Chem. Soc. Rev.*, 2012, **41**, 2172–2192.
13 F. Li, D.-M. Tang, Y. Chen, D. Golberg, H. Kitaura, T. Zhang, A. Yamada and H. Zhou, *Nano Lett.*, 2013, **13**, 4702–4707.
14 E. Yilmaz, C. Yogi, K. Yamanaka, T. Ohta and H. R. Byon, *Nano Lett.*, 2013, **13**(10), 4679–4684.
15 P. Tan, W. Shyy, T. S. Zhao, X. B. Zhu and Z. H. Wei, *J. Mater. Chem. A*, 2015, **3**, 19042–19049.
16 W. Zhou, Y. Cheng, X. Yang, B. Wu, H. Nie, H. Zhang and H. Zhang, *J. Mater. Chem. A*, 2015, **3**, 14556–14561.
17 B. Wu, H. Zhang, W. Zhou, M. Wang, X. Li and H. Zhang, *ACS Appl. Mater. Interfaces*, 2015, **7**, 23182–23189.
18 J. Zhang, Y. Zhao, X. Zhao, Z. Liu and W. Chen, *Sci. Rep.*, 2014, **4**, 6005–6010.
19 M. Hong, H. C. Choi and H. R. Byon, *Chem. Mater.*, 2015, **27**, 2234–2241.

20 Y. Cao, M.-s. Zheng, S. Cai, X. Lin, C. Yang, W. Hu and Q.-f. Dong, *J. Mater. Chem. A*, 2014, **2**, 18736–18741.
21 X. Lin, L. Zhou, T. Huang and A. Yu, *J. Mater. Chem. A*, 2013, **1**, 1239–1245.
22 S. H. Liu, Z. Y. Wang, C. Yu, Z. B. Zhao, X. M. Fan, Z. Ling and J. S. Qiu, *J. Mater. Chem. A*, 2013, **1**, 12033–12037.
23 J.-J. Xu, Z.-L. Wang, D. Xu, F.-Z. Meng and X.-B. Zhang, *Energy Environ. Sci.*, 2014, **7**, 2213–2219.
24 F. Li, D.-M. Tang, T. Zhang, K. Liao, P. He, D. Golberg, A. Yamada and H. Zhou, *Adv. Energy Mater.*, 2015, **5**, 1500294.
25 L. Zhang, L. Shi, L. Huang, J. Zhang, R. Gao and D. Zhang, *ACS Catal.*, 2014, **4**, 1753–1763.
26 L. Hu and Q. Chen, *Nanoscale*, 2014, **6**, 1236–1257.
27 L. Hu, P. Zhang, H. Zhong, X. Zheng, N. Yan and Q. Chen, *Chem.–Eur. J.*, 2012, **18**, 15049–15056.
28 X.-Y. Yu, L. Yu, H. B. Wu and X. W. Lou, *Angew. Chem., Int. Ed.*, 2015, **54**, 5331–5335.
29 J. Zhang, Y. Luan, Z. Lyu, L. Wang, L. Xu, K. Yuan, F. Pan, M. Lai, Z. Liu and W. Chen, *Nanoscale*, 2015, **7**, 14881–14888.
30 J. Zhang, L. Wang, L. Xu, X. Ge, X. Zhao, M. Lai, Z. Liu and W. Chen, *Nanoscale*, 2015, **7**, 720–726.
31 Y. Cui, Z. Wen and Y. Liu, *Energy Environ. Sci.*, 2011, **4**, 4727–4734.
32 J. Zeng, C. Francia, J. Amici, S. Bodoardo and N. Penazzi, *J. Power Sources*, 2014, **272**, 1003–1009.
33 J. Zhu, X. Ren, J. Liu, W. Zhang and Z. Wen, *ACS Catal.*, 2015, **5**, 73–81.
34 F. Wang, Z. Wen, C. Shen, K. Rui, X. Wu and C. Chen, *J. Mater. Chem. A*, 2015, **3**, 7600–7606.
35 M. Hu, S. Ishihara, K. Ariga, M. Imura and Y. Yamauchi, *Chem.–Eur. J.*, 2013, **19**, 1882–1885.
36 M. Hu, N. L. Torad and Y. Yamauchi, *Eur. J. Inorg. Chem.*, 2012, **2012**, 4795–4799.
37 Y. Li, B. Tan and Y. Wu, *J. Am. Chem. Soc.*, 2006, **128**, 14258–14259.
38 Y. Li and Y. Wu, *Chem. Mater.*, 2010, **22**, 5537–5542.
39 L. Zhang, H. B. Wu and X. W. Lou, *J. Am. Chem. Soc.*, 2013, **135**, 10664–10672.
40 Y. Tan, Q. Gao, C. Yang, K. Yang, W. Tian and L. Zhu, *Sci. Rep.*, 2015, **5**, 12382.
41 S. Zhang, J.-j. Shan, Y. Zhu, A. I. Frenkel, A. Patlolla, W. Huang, S. J. Yoon, L. Wang, H. Yoshida, S. Takeda and F. Tao, *J. Am. Chem. Soc.*, 2013, **135**, 8283–8293.
42 W.-H. Ryu, T.-H. Yoon, S. H. Song, S. Jeon, Y.-J. Park and I.-D. Kim, *Nano Lett.*, 2013, **13**, 4190–4197.
43 Y. Qin, J. Lu, P. Du, Z. Chen, Y. Ren, T. Wu, J. T. Miller, J. Wen, D. J. Miller, Z. Zhang and K. Amine, *Energy Environ. Sci.*, 2013, **6**, 519.